

1 **Analysis and comparison of the Core-to-Valence Luminescence mechanism in a large CLYC crystal**
2 **under neutron and γ -ray irradiation through optical filtering selection of the scintillation light**

3 F. Ferrulli^{1,2,*}, M. Caresana³, F. Cova⁴, S. Gundacker^{2,^}, N. Kratochwil^{2,5}, R. Pots², M. Silari², A. Vedda⁴, I.
4 Veronese⁶, G. Zorloni^{2,3}

5 ¹ *Université de Caen Normandie, 14032 CAEN 5, France*

6 ² *CERN, 1211 Geneva 23, Switzerland*

7 ³ *Department of Energy, Polytechnic of Milan, via Lambruschini 4, 20156, Milan, Italy*

8 ⁴ *Department of Materials Science, University of Milano – Bicocca, via Cozzi 55, 20125, Milan, Italy*

9 ⁵ *University of Vienna, Universitaetsring 1, 1010 Vienna, Austria*

10 ⁶ *Department of Physics, University of Milan and INFN, via Celoria 16, 20133, Milan, Italy*

11 * *Corresponding author*

12 [^] *Present address: Department of Physics of Molecular Imaging Systems, Institute for Experimental*
13 *Molecular Imaging, RWTH Aachen University, Forckenbeckstrasse 55, 52074 Aachen, Germany.*

14

15 **Abstract**

16 ⁷Li enriched Cs₂LiYCl₆:Ce³⁺ (CLYC) is a promising inorganic scintillator for real-time γ -ray and fast
17 neutron spectrometry. The neutron/ γ -ray discrimination is usually accomplished exploiting the
18 different quenching effects of high Linear Energy Transfer (LET) particles on different scintillation
19 mechanisms, usually by means of the time analysis of the pulse shape. In principle, the emission
20 wavelength information could be used to address the same task. However, a systematic study of the
21 correlations between the CLYC decay time, its radio-luminescence spectrum and the LET of the
22 impinging particle has not yet been performed. We therefore investigated the CLYC scintillation
23 process under neutron and γ -ray irradiation, correlating the time response to the scintillation
24 wavelength spectrum using a 1-inch right cylinder > 99% ⁷Li enriched CLYC. We found that the relative
25 intensity of the Core to Valence Luminescence (CVL) is almost constant with photons in the energy
26 range 20–660 keV, *i.e.* 0.5–5 keV/ μ m LET, and is only partially quenched by neutrons. Instead, the
27 direct electron-hole capture scintillation mechanism is completely cut under neutron irradiation. The
28 luminescence in between the deep-Ultraviolet and the Near Ultraviolet region (250-350 nm) might be
29 attributed to both the CVL and the host luminescence, also in thick highly Ce³⁺-doped crystals.

30 **Keywords** – CLYC, Core to Valence Luminescence, wavelength-based discrimination, pulse shape
31 analysis, radioluminescence, Time Correlated Single Photo Counting

32 **1. Introduction**

33 The Cs₂LiYCl₆:Ce³⁺ (CLYC) is a promising inorganic scintillator for γ -ray spectrometry and neutron
34 detection, with good neutron/ γ -ray (n/ γ) discrimination capability. CLYC rather good γ -ray
35 spectrometry capabilities are due to its density (3.3 g/cm³), Z_{eff} (54) and energy resolution, about 5%
36 at 662 keV [1,2]. Its fast neutron spectrometry properties were recently demonstrated for ⁷Li enriched
37 crystals [3,4]. The reactions involved are ³⁵Cl(n,p)³⁵S and ³⁵Cl(n, α)³²P below 15 MeV. The n/ γ
38 discrimination can be performed through Pulse Shape Discrimination (PSD) by exploiting the different
39 decay times of the scintillator when irradiated with neutrons and photons.

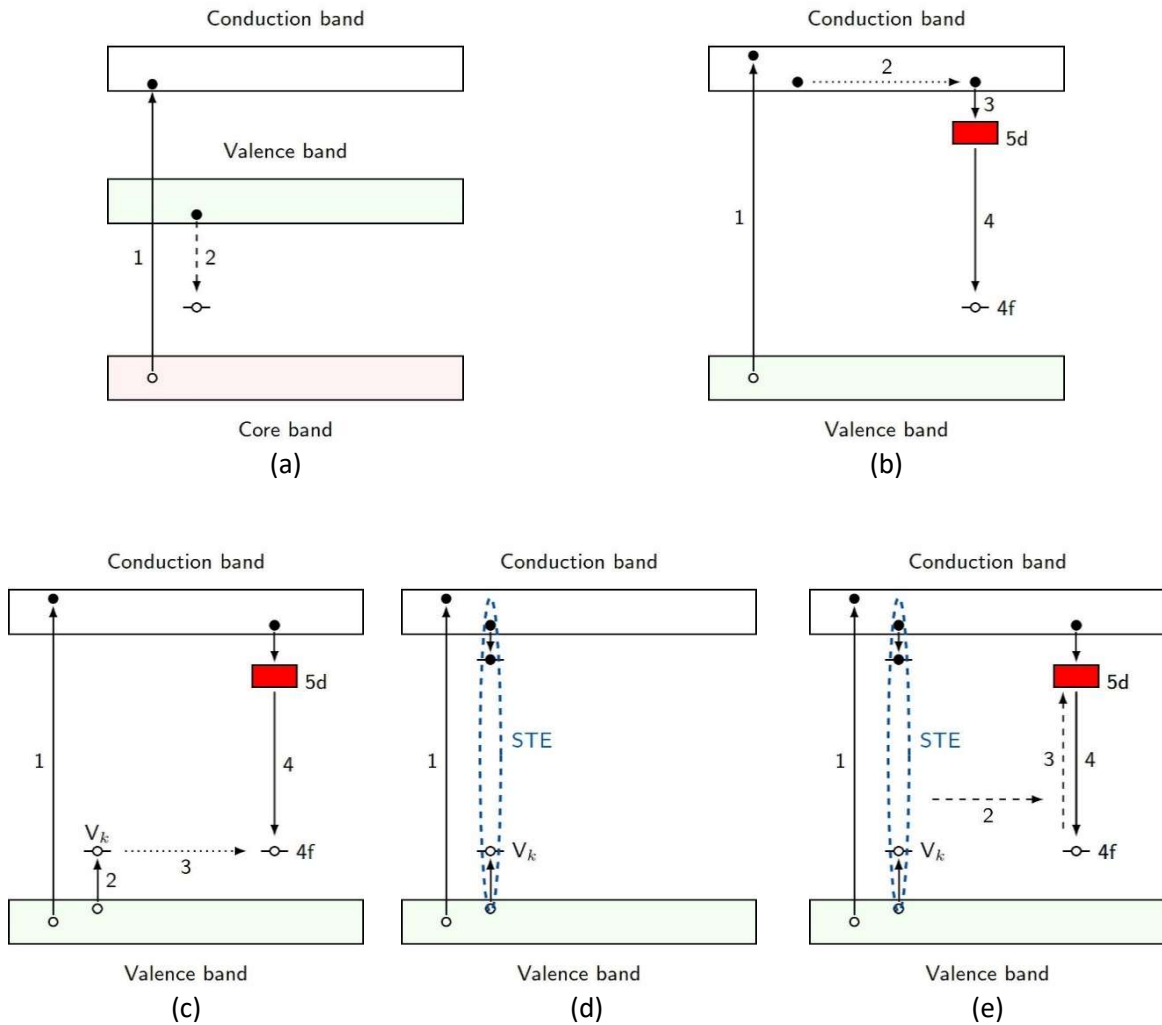
40 The good PSD capability of CLYC is mainly ascribed to the presence of the Core-To-Valence
41 Luminescence (CVL) [5], a scintillation mechanism that, according to the literature, is selectively
42 quenched by high Linear Energy Transfer (LET) particles, such as the reaction products emitted after
43 neutron capture on ^{35}Cl [4,6]. These reaction products completely quench the CVL mechanism, causing
44 a different time profile of the de-excitation process (and consequently of the detected signal) when
45 the crystal is excited by neutrons rather than by γ -rays.

46 The CVL (also called cross-luminescence or Auger free luminescence) is an ultra-fast mechanism where
47 an electron from the core band is excited into the conduction band. The consequent hole produced in
48 the core band recombines with an electron of the valence band. Since the valence band is filled with
49 electrons, the recombination probability is large resulting in a fast process [7]. The CVL is a competitive
50 radiative de-excitation process with a decay time faster than that of the other three scintillation
51 mechanisms present in CLYC, described below [8,9]. In CLYC, the CVL has a decay time of the order of
52 1-5 ns and is characterized by the emission of photons in between the deep-Ultraviolet (UV) and Near
53 Ultraviolet (NUV) region (225-330 nm) [10,11]. The fast (direct electron-hole capture) and
54 intermediate (binary electron-hole recombination mediated by the formation of a trapped hole
55 centre, usually called V_k complex [12]) mechanisms are related to the Ce^{3+} de-excitation, and are
56 characterized by a decay time of the order of 50 ns and 500 ns respectively. Both the fast and
57 intermediate mechanism emit in the Ce^{3+} -related spectral range, *i.e.* between 350 nm and 450 nm [9].
58 The slowest mechanism is related to the host luminescence, with the formation of the so called self
59 trapped excitons (STEs), and is characterized by a decay time of several μs [11,12]. In doped thick
60 crystals, the STEs preferentially de-excite on Ce^{3+} , hence in the range 350-450 nm, but the decay
61 constant is still governed by the STE migration dynamics, with a half life of a few microseconds [12].
62 Figure 1 shows a schematic of the energy levels of each scintillation mechanism (plots (c), (d) and (e)
63 were taken from [12]). Plot (a) shows the CVL, plot (b) the fast Ce^{3+} emission, usually ascribed to γ -ray
64 irradiation only. Plot (c) shows the intermediate mechanism, *i.e.* the V_k centre transferring its energy
65 to the Ce^{3+} . The STE is represented both as a luminescence centre itself (plot (d)) and when it transfers
66 its energy to the Ce^{3+} (plot (e)).

67 Since the CVL emission occurs in a different spectral region than the Ce^{3+} de-excitation, in principle
68 the spectral information can be used to perform particle discrimination [13–15]. Considering that
69 the CVL is observed only under photon irradiation, a CVL-selective optical filter should allow
70 distinguishing a photon-induced signal from a neutron-induced one. However, a systematic study of
71 the correlations between the CLYC decay time, its spectral information and the LET of the impinging
72 particle has not yet been performed.

73
74 We therefore investigated the CVL behavior when the crystal is excited by neutrons and photons,
75 correlating the time response to the scintillation wavelength spectrum. The analysis was carried out
76 following two different methods: 1) by measuring the X-ray and γ -ray excited radio-luminescence (RL)
77 spectra at different photon energies, and 2) by performing a pulse shape analysis of the signal
78 produced by the interaction of γ -rays and neutrons, using both a photomultiplier tube (PMT) and a
79 Time Correlated Single Photon Counting (TCSPC) technique [16,17]. All measurements were repeated
80 with and without an optical filter in between the crystal and the sensor. The filter was chosen to select
81 only the CVL-related spectral region. This allowed investigating the effects of the LET of the impinging
82 particles on the specific scintillation mechanisms.

83



84

85 *Figure 1. Scintillation mechanisms in CLYC [12]. (a) Excitation of an electron from the core band to the*
 86 *conduction band and subsequent formation of a hole (1); the hole in the core band then recombines*
 87 *with a valence electron (2) causing the emission of the CVL light. (b) Excitation of an electron from the*
 88 *valence to the conduction band (1); the electron then migrates (2), reaching a Ce³⁺ recombination site*
 89 *(3), with the subsequent radiative de-excitation (4). (c) Excitation of an electron from the valence*
 90 *to the conduction band (1) leaving a hole in the valence band; the hole is then trapped in a positive V_k*
 91 *centre, forming a Cl₂⁻ molecular complex (2). This defect thermally migrates (3) to a Ce³⁺ centre forming*
 92 *a Ce⁴⁺ or a Ce³⁺ + V_k complex. Eventually, the new centre recombines with an electron from the*
 93 *conduction band (4). (d) Excitation of an electron from the valence to the conduction band and*
 94 *formation of a V_k complex (1); a free electron is then trapped forming a STE complex, which can*
 95 *recombine radiatively. (e) After the formation of the STE (1), this complex thermally migrates to a Ce³⁺*
 96 *centre (2). The STE can de-excite transferring its energy to a Ce³⁺ centre (3), which subsequently*
 97 *recombines (4).*

98 **2. Materials and methods**

99 The measurements were performed with a 1-inch right cylinder CLYC scintillator enriched in ⁷Li to >
 100 99%, purchased from Radiation Monitoring Devices [18]. The crystal is hygroscopic and therefore
 101 encapsulated in an aluminum housing provided with a single quartz window. The filter employed is an
 102 Asahi Spectra XUV0325 Shortpass Optical filter (∅ 25 mm, wavelength cut-off 325 nm) [19]. Its

103 transmittance was measured with an Agilent Varian Cary 50 spectrophotometer ranging from 190 nm
104 to 1100 nm.

105 **2.1 Radio-luminescence measurement setup**

106 The first RL measurements were performed at the University of Milano – Bicocca. The measurement
107 system is made of a liquid nitrogen-cooled, back-illuminated and UV-enhanced charge-coupled device
108 (CCD) (Jobin-Yvon Spectrum One 3000). The CCD is coupled with a monochromator (Jobin-Yvon Triax
109 180) with a 100 grooves/mm grating. The RL excitation was obtained by X-ray irradiation using a Philips
110 PW2274 X-ray tube with a tungsten anode and a Be-window, operated at 20 kV.

111 The second set of measurements employed a portable Back-thinned CCD Array Spectrometer Prime X
112 (B&W TEK) [20]. A portable device was used for the irradiations performed at the calibration
113 laboratory of the Polytechnic of Milan. X-ray fields were produced via a high-stability Seifert ISOVOLT
114 320/10 X-ray generator (maximum voltage 300 kV). The tube provides the complete ISO 4037 standard
115 X-ray series radiation qualities [21]. In particular, the quasi-monoenergetic Narrow series (N-series)
116 were employed. The N-series radiation qualities are recommended for the study of the energy
117 dependence of the response of dosimeters [21]. γ -ray fields were produced by a certified 370 GBq
118 ^{137}Cs isotopic source. The scintillation light emitted by the crystal was sent to the spectrometer
119 through an optical fiber cable. The fiber and the crystal were coupled using a black cone and a tailored
120 3D printed assembly to optimize the light collection and reduce the light losses. The spectrometer was
121 controlled via a laptop.

122 **2.2 Setup with the ultra-fast H6610 Hamamatsu PMT**

123 For the analysis of the CVL time behavior, the Hamamatsu H6610 Bialkali PMT was selected for both
124 its time response and its spectral response [22]. According to its datasheet, at 25 °C the PMT is
125 characterized by a rise time of 0.7 ns and by a transit time spread of 0.16 ns. These values must be
126 compared to the characteristic decay constants of the CLYC scintillation process. The observed shape
127 of the electric signal on an oscilloscope coupled to the PMT is indeed given by the convolution of the
128 time response of the PMT itself and the decay time of the scintillator. In this case, the contribution of
129 the PMT can partially influence the precise determination of the CVL decay time (0.7 ns *versus* 1–5 ns)
130 but for the other scintillation mechanisms its influence is completely negligible, as they all decay with
131 half life > 50 ns.

132 Besides being characterized by a very short decay time, the CVL mechanism is observed in between
133 the deep-UV and NUV wavelength range (250-350 nm). The quantum efficiency of the H6610 PMT
134 varies from about 10% to 20% from roughly 200 nm up to 430 nm [22]. The window material of the
135 H6610 PMT is made of silica glass, which transmits ultraviolet light down to 160 nm. On the contrary,
136 the window material of commonly used PMTs consists of borosilicate glass, which transmits light only
137 down to 300 nm [23]. The CLYC was coupled to the H6610 PMT through an optical grease (Rhodorsil
138 Pate 7). The effective area of the PMT photocathode (20 mm diameter) was completely covered by
139 the crystal surface whose diameter is 25.4 mm. The PMT was supplied with -2500 V, and the output
140 connected to a Teledyne LeCroy Waverunner 8104 Oscilloscope (1 GHz, 20 GSamples/s) with a 50 Ω
141 termination. The PMT and the crystal were placed inside a light-tight and thermally regulated chamber
142 kept at 18 °C. When the optical filter was interposed between the PMT photocathode and the CLYC, a
143 thin layer of the optical grease was applied on both surfaces of the filter for optical coupling.

144 The irradiations were performed employing a ^{137}Cs source (3.31 MBq) and an unshielded Am-Be
145 neutron source (359.03 MBq).

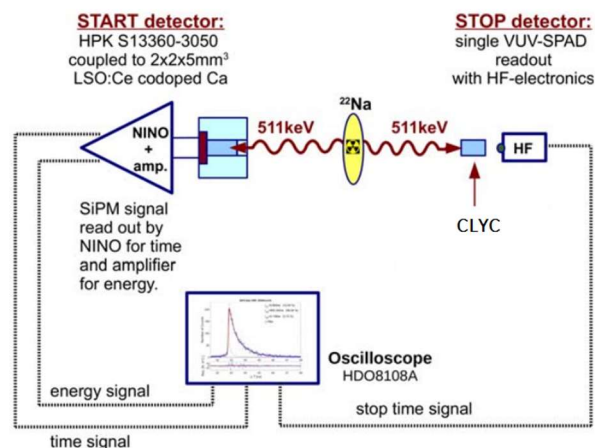
146 **2.3 Time Correlated Single Photo Counting (TCSPC) setup**

147 The TCSPC technique is specifically aimed for precise rise and decay time measurements of inorganic
148 scintillators [16,17]. A ^{22}Na β^+ source was interposed between the CLYC and a fast detection system
149 called start detector. The start detector is composed of a 2 mm \times 2 mm \times 5 mm LSO:Ce crystal coupled
150 to an Hamamatsu Photonics K.K. (HPK) S13360-3050 Silicon Photomultiplier (SiPM) with a Meltmount
151 thermoplastic, connected to a NINO readout board [24]. On the other side, the CLYC faced a Vacuum
152 Ultraviolet single-photon avalanche diode (VUV-SPAD) from Fondazione Bruno Kessler, called stop
153 detector ([25]). A SPAD is a photodiode operating in Geiger mode as an on-off switch triggered by a
154 photon arriving on its surface. A SiPM is actually a dense array of independent SPADs, whose function
155 is to count the number of photons reaching the SiPM surface [26]. In the hereby described setup, the
156 CLYC and the stop detector (the VUV-SPAD) were not optically coupled [27].

157 The TCSPC technique works as follows (Figure 2). When one of the two annihilation γ -rays emitted in
158 coincidence by the source is detected in the start detector, the time measurement starts. If the second
159 γ -ray interacts with the crystal facing the stop detector, the scintillation produces several visible
160 photons following its characteristic decay time statistics. The time measurement stops when the first
161 scintillation photon reaches the stop detector. Saving a large number of events and plotting them on
162 a histogram, the decay time of the scintillator is reconstructed in terms of number of counts *versus*
163 emission time [16,17].

164 The measurement was performed with and without the filter. In the former case, the filter was
165 interposed between the CLYC and the stop detector, at a distance of a few centimeters from both.
166 Because of the smaller dimensions of the stop detector (a few tens of μm^2) compared to the surface
167 of the filter (\varnothing 25 mm), it is reasonable to assume that the light reaching the photodetector was
168 correctly filtered.

169



170

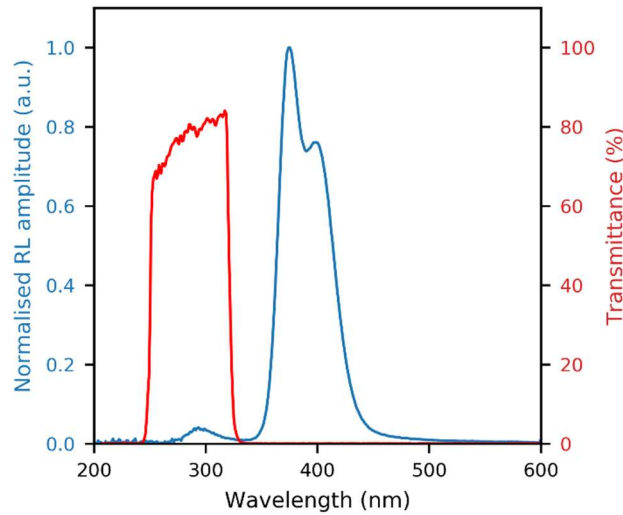
171 *Figure 2. The TCSPC setup with the CLYC crystal [27].*

172 **3. Results and discussion**

173 **3.1 Radioluminescence spectra**

174 Figure 3 shows the results of the RL characterization of the crystal performed at the University of
175 Milano - Bicocca. The X-ray tube was operated at 20 kV. The RL emission spectrum was corrected for
176 the background and for the spectral response of the detection system. The resulting spectrum shows
177 the characteristic doublet peak due to the Ce^{3+} emission in the 340-500 nm range, peaked at 375 nm

178 and 395 nm. A band is also revealed at around 300 nm, which is usually attributed to the CVL
 179 scintillation mechanism [8,28]. The relative intensity of the CVL mechanism with respect to the total
 180 scintillation light was quantified as the ratio of the area under the CVL portion of the spectrum
 181 (between 260 nm and 330 nm) over the area under the entire emission spectrum (between 260 nm
 182 and 500 nm). The CVL contribution is about 5% of the total signal. Figure 3 also shows the filter
 183 transmittance. It can be observed that the filter is selective to the CVL emission and completely cuts
 184 the Ce^{3+} emission region.

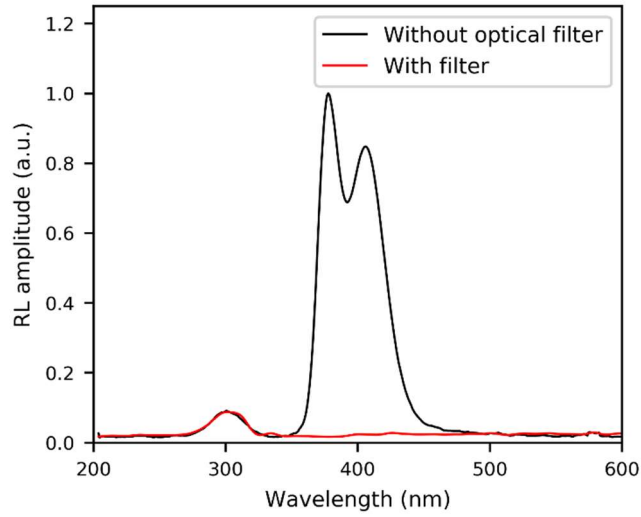


185
 186 *Figure 3. Left y-axis: RL emission spectrum in CLYC irradiated with the X-ray tube operated at 20 kV.*
 187 *Right y-axis: measured transmittance of the Asahi Shortpass filter.*

188 Figures 4 and 5 show the results obtained at the Polytechnic of Milan. The spectra are background
 189 corrected and normalized to their maximum. The background was calculated as the average value of
 190 counts in the 800-900 nm region. The spectra are not corrected for the spectral response of the
 191 detector, because the response of the CCD was not characterized below 350 nm. However, a
 192 comparison in relative terms is still valid since the experimental setup was the same for all irradiations
 193 performed at the Polytechnic.

194 Figure 4 shows the RL spectra measured irradiating the CLYC with the ^{137}Cs source with and without
 195 the optical filter. The measurement demonstrates the proper selectivity of the filter in cutting the
 196 Ce^{3+} -related emission. Figure 5 shows the RL spectra obtained irradiating the crystal at different X-ray
 197 energies and with ^{137}Cs photons. Most authors working on the CLYC characterization generally agree
 198 that the CVL mechanism is selectively quenched only by high-LET particles such as neutron capture
 199 products. However, to the best of our knowledge the LET dependence of the RL spectral emission
 200 under γ -ray irradiation has never been studied. If a dependence of the CVL on LET in the tested 0.5–
 201 5 keV/ μm range exists, the shape of the scintillation spectrum must vary as a function of the photon
 202 energy. Figure 6 shows the LET versus photon energy in the selected energy range.

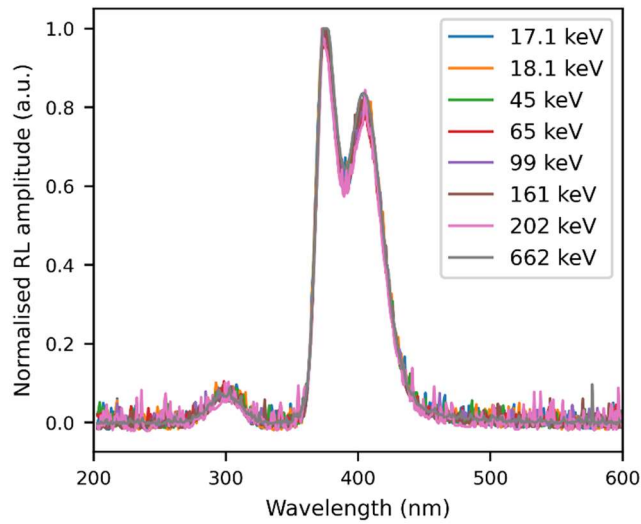
203 If a dependence exists, methods based on the CVL suppression for neutron identification might return
 204 wrong results, *i.e.* low-energy photon-induced events could be misinterpreted as neutron-induced
 205 ones. This should be particularly critical in the case of a system using an optical-based discrimination
 206 readout. The curves shown in figure 5 do not reveal any dependence of the CVL mechanism on the
 207 energy of the incident photons.



208

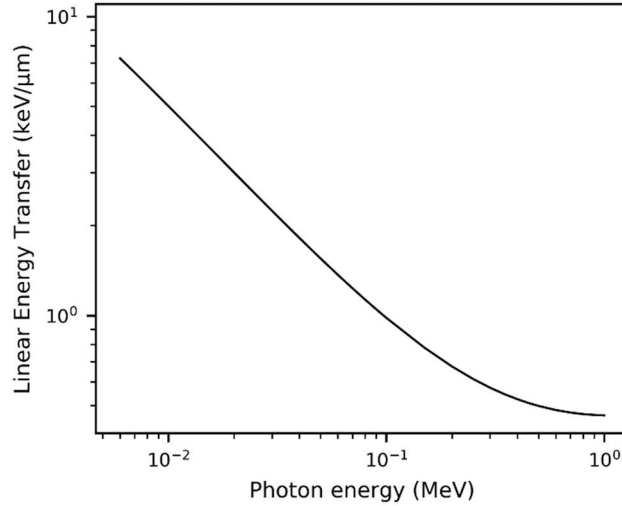
209 *Figure 4. RL emission spectrum in CLYC irradiated with the ^{137}Cs source, measured with and without the*
 210 *Asahi Shortpass filter between the crystal and the optical fiber.*

211



212

213 *Figure 5. Normalized RL emission spectra of CLYC irradiated with X-rays of different energies (mean*
 214 *values between 17.1 keV and 202 keV) and with the ^{137}Cs source (662 keV).*



215

216 *Figure 6. The LET versus photon energy calculated for the CLYC crystal in the 5 keV – 1 MeV energy*
 217 *region. Data taken from [29].*

218 RL measurements under neutron irradiation were undertaken using an 888 GBq Am-Be fast neutron
 219 source at CERN. The employed readout setup was the same as the one used at the Polytechnic of
 220 Milan. A 5 cm thick lead slab was interposed between the neutron source and the crystal to suppress
 221 the γ -ray background. In spite of the relatively high activity of the source, the low ^{35}Cl capture cross
 222 section and the low sensitivity of the portable spectrometer prevented the detection of any signal
 223 above the instrument noise.

224 3.2 Pulse shape analysis with the ultra-fast H6610 Hamamatsu PMT

225 The time information was obtained employing the Hamamatsu H6610 PMT. Four experiments were
 226 performed: ^{137}Cs irradiation in bare configuration (*i.e.* CLYC facing the PMT), ^{137}Cs irradiation in filtered
 227 configuration (*i.e.* with the optical filter placed between CLYC and PMT), Am-Be irradiation in bare
 228 configuration and Am-Be irradiation in filtered configuration.

229 In the case of the photon irradiation, all pulses were analyzed by aligning, normalizing and averaging
 230 the data under the ^{137}Cs photopeak at 662 keV, thus obtaining the so-called standard pulse. In the
 231 case of Am-Be irradiation, particle discrimination was first performed by PSD using the charge
 232 integration method [30]. The collected signals were integrated following the formula:

$$233 \text{ PSD} = \frac{Q_{\text{prompt}}}{Q_{\text{prompt}} + Q_{\text{tail}}} \quad (1)$$

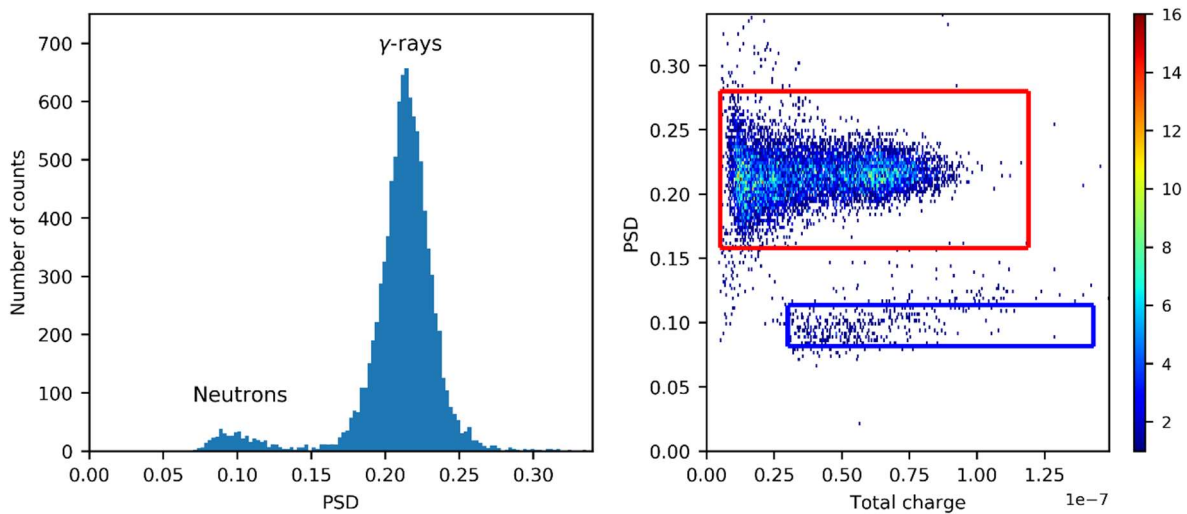
234 where Q_{prompt} is the integral charge between the start of integration and 50 ns, and Q_{tail} is the
 235 integral charge from 50 ns to 1500 ns. These two values were chosen after the optimization of the PSD
 236 Figure Of Merit (FOM = 2.33). The FOM was calculated as following [24]:

$$237 \text{ FOM} = \frac{x_{\gamma} - x_n}{FWHM_{\gamma} + FWHM_n} \quad (2)$$

238 where x_{γ} and x_n are the mean values of the photon and neutron gaussian distributions of the PSD
 239 and $FWHM_{\gamma}$ and $FWHM_n$ the corresponding full widths at half maximum.

240 Figure 7 shows the PSD histogram plot, from which the FOM was calculated, and the 2D histogram
 241 plot of the PSD versus the total charge in the case of unfiltered Am-Be irradiation. The acquired signals

242 were then classified in the PSD space, and only those belonging to the neutron region of the PSD space
 243 (blue box in the right plot of figure 7) were used for the decay time analysis. The neutron region was
 244 defined by the signals with a PSD value within $x_n \pm \sigma_n$, i.e. between 0.082 and 0.113, in order to cut
 245 the signals in the tails of the Gaussian distribution.
 246 For the sake of completeness, also the signals classified in the PSD space as photons (red box in the
 247 right plot of figure 7) were averaged and the corresponding standard pulse was calculated for the
 248 decay time analysis.
 249 The uncertainty of the calculated decay time is mainly affected by the number of the averaged signals,
 250 the signal alignment and the region selected as neutrons or photons in the 2D PSD histogram plot,
 251 whereas the uncertainty on the fitting procedure is negligible. A total uncertainty of 10 % was
 252 estimated for the measurements with the PMT.
 253



254
 255 *Figure 7. On the left, the PSD histogram plot calculated for the Am-Be neutron source; on the right, the*
 256 *2D PSD histogram plot where γ -rays and neutrons are identified by the two regions enclosed in a red*
 257 *and a blue box, respectively.*

258 As mentioned above, measurements were performed for both the bare and the filtered configuration.
 259 However, the filtered results had to be discarded, because the filter did not significantly modify the
 260 recorded signals in the case of both γ -ray and neutron irradiations. This result is in contrast with the
 261 previous RL measurements, where it was observed that only the emission related to the CVL region
 262 was transmitted by the optical filter, and thus an appreciable distortion of the signal was expected.
 263 Moreover, the signal amplitude did not vary significantly. Therefore, the filtered results were rejected
 264 because of experimental errors (two possible explanations are given in section 4), and hereafter only
 265 the unfiltered configuration results are discussed.

266 The decay curves of the standard pulses were fitted using a sum of four, for γ -rays, and three, for
 267 neutrons, exponential decays, according to the following equation:

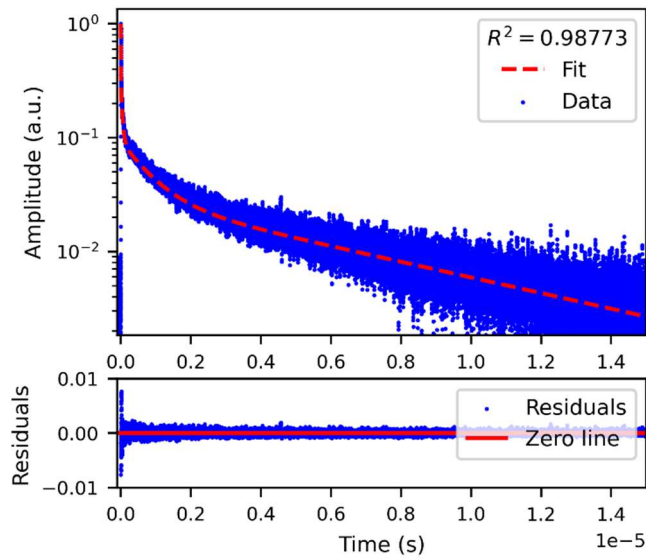
$$268 \quad y(t) = \sum_i A_i e^{-t/\tau_i} \quad (3)$$

269 where A_i is the amplitude of each exponential and τ_i the decay time.

270 Figures 8, 9 and 10 show the standard pulses with the fit and the plot of the residuals calculated as
 271 the difference between the experimental and the model predictions. In all cases the fit is satisfactory,
 272 with $R^2 \sim 1$; the model does not systematically underestimate/overestimate the experimental data.
 273 The results of the fits are summarized in table 1. The uncertainties reported in table 1 are statistical.

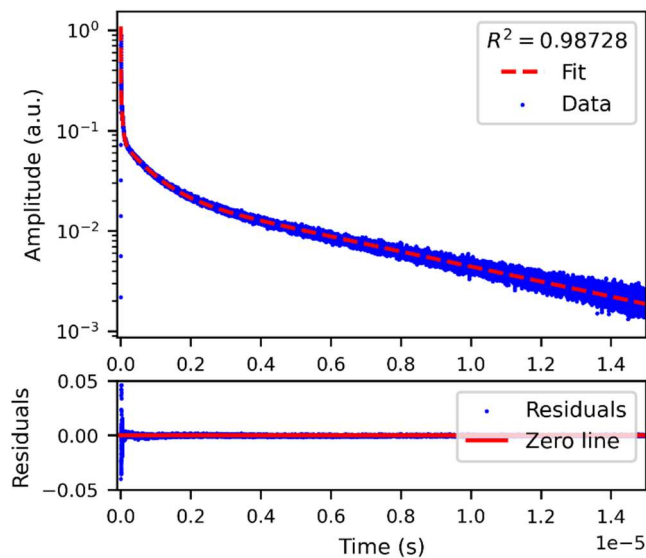
274 For each pulse, the table reports the time constants τ_i and the relative intensity of the associated
275 scintillation mechanism in relation to the total signal. The relative intensities were calculated as the
276 percent contribution of the single scintillation mechanism to the total signal.

277



278

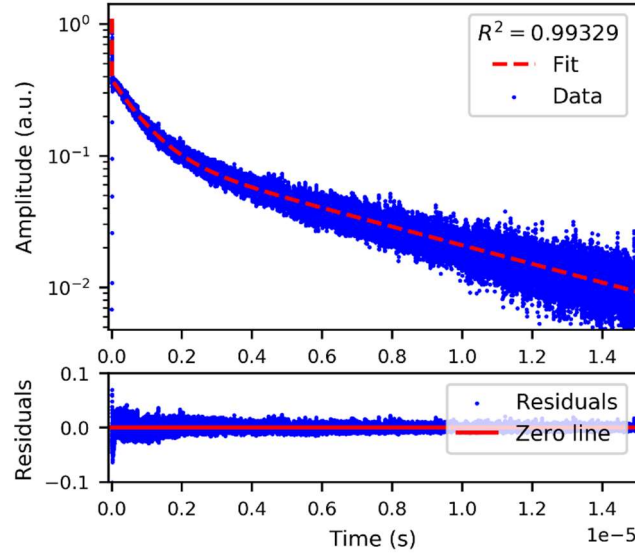
279 *Figure 8. Top: the standard pulse and the fit of the photon signals for the ¹³⁷Cs source irradiation.*
280 *Bottom: the plot of the residuals.*



281

282 *Figure 9. Top: the standard pulse and the fit of the photon signals for the Am-Be source irradiation.*
283 *Bottom: the plot of the residuals.*

284



285

286 *Figure 10. Top: the standard pulse and the fit of the neutron signals from the Am-Be source irradiation.*

287 *Bottom: the plot of the residuals.*

288

289 *Table 1. The decay times (τ) and the relative intensity (Int) of the CLYC scintillation mechanisms*
 290 *calculated for the standard pulses produced by γ -rays and neutrons. Measurements performed with*
 291 *the Hamamatsu H6610 PMT.*

292

Particle (source)	CVL		Fast Ce ³⁺		V _k		STE		R ²
	τ_1 (ns)	Int (%)	τ_2 (ns)	Int (%)	τ_3 (ns)	Int (%)	τ_4 (ns)	Int (%)	
γ -rays (¹³⁷ Cs)	2.7 ± 0.3	1.10	45 ± 5	3.26	781 ± 78	20.68	6325 ± 633	74.96	0.988
γ -rays (Am-Be)	2.5 ± 0.2	1.49	43 ± 4	3.70	747 ± 75	21.11	5806 ± 581	73.70	0.997
Neutrons (Am-Be)	1.7 ± 0.2	0.22	—	—	824 ± 82	25.57	6140 ± 614	74.21	0.993

293

294 As expected, for the γ -ray irradiation four mechanisms were observed, with their estimated
 295 coefficients in agreement with the literature, *i.e.* CVL 1-5 ns, direct capture \sim 50 ns, binary
 296 recombination mediated by V_k \sim 700 ns and STE \sim 5 μ s. In general, literature data agree on the
 297 quenching effects of high LET particles on the CVL. The LET of an α particle produced by a neutron
 298 reaction from an Am-Be source in CLYC is around 150 keV/ μ m while it is 15 keV/ μ m for a proton, *i.e.*
 299 30 and 3 times higher, respectively, than the maximum LET studied in section 3.1. However, the
 300 present results show that an ultra-fast scintillation mechanism is also present with neutrons, which
 301 was attributed to the CVL. The faster decay time of the CVL with neutrons might be due to the
 302 statistical uncertainty of the standard pulse. Nevertheless, a fast decay component is clearly seen from
 303 the neutron standard pulse (see figure 10).

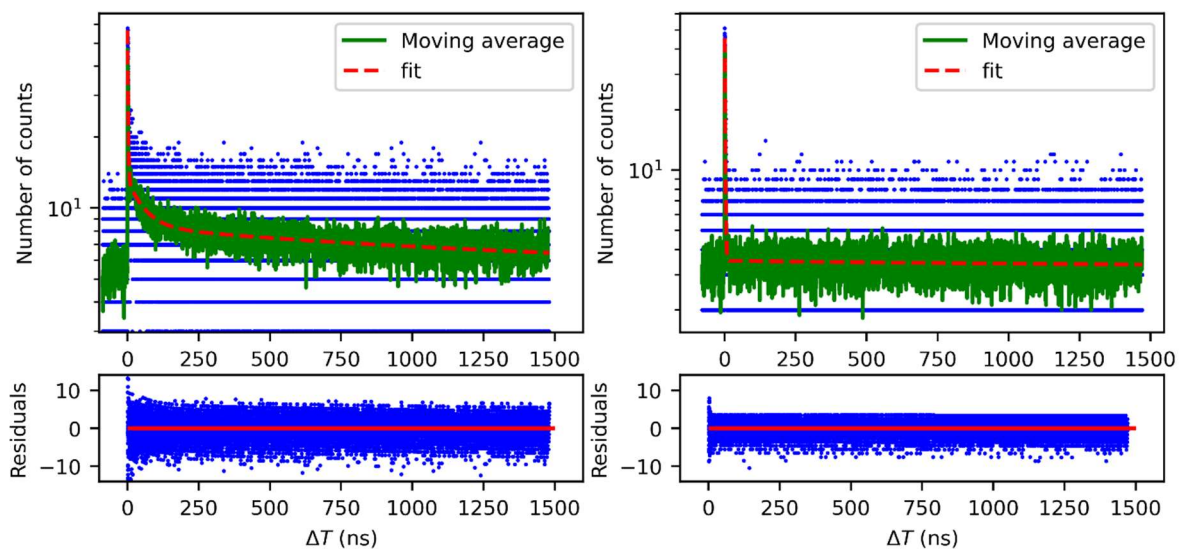
304 According to the present results, the CVL is only partially quenched by neutrons, while the fast decay
 305 is completely quenched. In fact, the neutron standard pulse is better fitted by a 3-exponential function
 306 rather than a 4-exponential one. The relative importance of the CVL drops from 1.1% with a 4-

307 exponential function in the case of γ -ray irradiation, down to 0.22% with a 3-exponential function in
 308 the case of neutron irradiation. This result is not in complete disagreement with literature data. Firstly,
 309 the CVL is actually quenched by high LET particles. In addition, the low intensity of the residual CVL
 310 might not be observed if the employed setup is not sensitive enough. In the present experiment, the
 311 flat spectral response and fast rise time of the Hamamatsu H6610 PMT together with the fast
 312 oscilloscope allowed distinguishing between the two contributions (CVL and fast Ce^{3+}) even in the case
 313 of a strong CVL quenching.

314 3.3 Pulse shape analysis with the Time Correlated Single Photo Counting (TCSPC) setup

315 Figure 11 shows the results of the TCSPC measurement: the left plot shows the unfiltered
 316 configuration, the right plot the filtered one. The points in the histogram are the time measurements
 317 with a bin width of 60 ps. The green line is the moving average of the data, the red line is the fit to the
 318 data. The plot of the residuals of each pulse is also shown. For a better analysis of the filtered data,
 319 figure 12 shows a zoom of the results for the filtered case together with the measured Impulse
 320 Response Function (IRF) of the system, *i.e.* the time resolution of the acquisition system. The fitting
 321 equation shown in figure 12 was obtained by convolving the IRF with the scintillator response function.
 322 The details of the fitting procedure are described in [17]. Figure 12 shows that the contribution of the
 323 IRF to the decay component of the measured pulse is negligible. Table 2 reports the decay times τ_d ,
 324 with their statistical uncertainties and their relative intensity on the total signal. A 0.5 % uncertainty
 325 on the calculation of the decay times is due to the TCSPC setup [16], which is negligible with respect
 326 to the fitting uncertainty. Thus, the latter is reported in table 2.

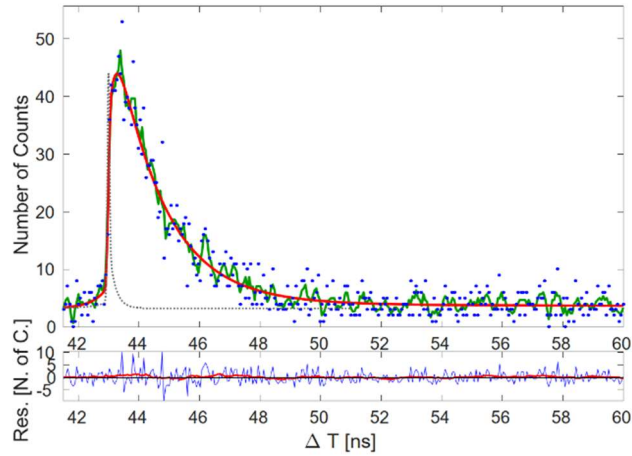
327



328

329 *Figure 11. The result of the TCSPC measurement of the CLYC response without the filter (on the left)*
 330 *and with the filter (on the right). The points are the measured data, the green line is the moving*
 331 *average and the red line is the fit. The bottom plots show the corresponding residuals.*

332



333

334 *Figure 12. A zoom of the results of the TCSPC measurement of the CLYC response with the filter. The*
 335 *points are the measured data, the green line is the moving average and the red line is the fit. The*
 336 *dotted black line is the IRF of the system.*

337 *Table 2. The decay times (τ) and the relative intensity (Int) of the CLYC scintillation mechanisms*
 338 *estimated through the TCSPC technique in both bare and filtered configurations.*

Setup	CVL		Fast Ce ³⁺		V _k + STE		χ^2
	τ_1 (ns)	Int (%)	τ_2 (ns)	Int (%)	τ_3 (ns)	Int (%)	
Unfiltered	1.90 ± 0.07	2.06	57 ± 4	6.53	1379 ± 67	91.41	1.002
Filtered	1.67 ± 0.04	18.58	—	—	1639 ± 482	81.42	0.997

339

340 The decay constants estimated with the TCSPC setup without the filter match reasonably well the
 341 decay times measured with the PMT and agree with literature data, taking into account the different
 342 recorded length [9,31]. In the filtered configuration the fast emission is dominated by the CVL
 343 mechanism, while the Ce³⁺ emission around 50 ns is not detected, so it appears that optical filtration
 344 is in line with the RL measurements.

345 The TCSPC setup is optimized for the estimation of the fastest decay mechanisms of the analyzed
 346 scintillator. In particular, its 60 ps discretization and the possibility to introduce the impulse response
 347 function of the measurement system in the fit allow precisely estimating extremely fast decay
 348 constants [17]. Conversely, the 1500 ns integration window does not permit distinguishing between
 349 the two slowest scintillation mechanisms, which are merged in a single V_k + STE component.

350 3.4 Discussion

351 The different experiments here reported aimed at observing the same scintillation process from
 352 different perspectives, *i.e.* in the time and wavelength domains. The RL filtered vs unfiltered results
 353 can be qualitatively compared to the TCSPC filtered vs unfiltered results, respectively. In both cases,
 354 the optical filter was placed at a certain distance between the crystal and the sensor without any
 355 optical coupling. The RL measurement results showed that no signal was collected at wavelengths
 356 longer than the filter cut-off. In the TCSPC experiments, the decay constant of the fast mechanism,
 357 which is confined within 350–450 nm wavelength range, completely disappeared.

358 The merged $V_k + \text{STE}$ component becomes appreciably slower with the optical filtration, thus
 359 suggesting that also the intermediate component, which is again confined in the Ce^{3+} -related region,
 360 was blocked by the filter. Literature data and the RL measurement (figure 3) endorse this hypothesis.
 361 Thus, the retention of the slower component in the filtered signal can be ascribed to the STE de-
 362 excitation since its emission spectrum spans from 240 nm up to 460 nm [11,12,32], even though in
 363 large doped crystals the STEs mainly de-excite on Ce^{3+} . Therefore, most of the signal belonging to the
 364 lower wavelength region appears to be dominated by STE de-excitation instead of CVL (at least > 80%
 365 relative importance; the exact value can be obtained with integration windows at least $\geq 15 \mu\text{s}$).
 366 However, the number of counts of the filtered signal in the tail region is around the background level
 367 and its estimation is affected by a major uncertainty. For this reason, the relative intensities of the
 368 decay mechanisms in the deep-UV – NUV region cannot be precisely evaluated.

369 The TCSPC and fast PMT results can be quantitatively compared. The H6610 PMT is particularly fast:
 370 its rise and transit times are of the order of tenths of ns. However, considering the 1–5 ns decay
 371 constant of the CVL, the PMT response function is expected to perturb the estimation of the decay
 372 constant. On the contrary, the 1500 ns integration window allowed distinguishing between the
 373 intermediate and the slow components.

374 Therefore, the two measurements allow estimating different quantities in the bare configuration
 375 under γ -ray irradiation, but a correspondence should first be established. To assess the
 376 correspondence between the two measurements, one can integrate the fast PMT measurement in
 377 the bare configuration under photon irradiation for 1500 ns and compare it to the corresponding
 378 TCSPC result. The fit has to be done with the same 3-exponential function of the TCSPC experiment.
 379 Table 3 summarizes the obtained fit coefficients with their statistical uncertainty and their relative
 380 intensities.

381 *Table 3: Decay constants (τ) and relative intensities (Int) of the CLYC scintillation mechanisms measured*
 382 *with the TCSPC technique compared to the Hamamatsu H6610 PMT results. In both cases the*
 383 *integration time was 1500 ns.*

Setup	CVL		Fast Ce^{3+}		$V_k + \text{STE}$	
	τ_1 (ns)	Int (%)	τ_2 (ns)	Int (%)	τ_3 (ns)	Int (%)
TCSPC	1.90 ± 0.07	2.06	57 ± 4	6.53	1379 ± 67	91.41
PMT	2.8 ± 0.3	2.04	49 ± 5	6.46	1394 ± 139	91.50

384

385 The two fits are quantitatively superimposable. The main difference is a 45% discrepancy on the CVL
 386 decay constant, which is slower in the case of the fast PMT measurement. The result was expected
 387 since the PMT response time is comparable to the CVL decay constant. However, the relative intensity
 388 is the same for the PMT and TCSPC measurements. Hence, the four decay coefficients estimated with
 389 the fast PMT measurement (see table 2) can be considered sufficiently accurate for estimating the
 390 effects of the neutron quenching on the CLYC scintillation mechanisms. Therefore, the conclusions
 391 drawn in section 3.2 are further validated, *i.e.* with neutrons the fast mechanism is fully quenched,
 392 while the CVL is strongly, but only partially, quenched.

393 It is worth mentioning that the quenching of the CVL by heavy ions is still under study, especially for
 394 relatively new crystals such as CLYC. Most of the authors agree with ascribing this effect to the high
 395 excitation density promoted by heavy ions [5,33,34], however its origin is not completely clear. For

396 example, according to Kirm et al., [33], the quenching of the CVL is due to the higher probability, with
397 increasing LET, of recombination between the electrons of the conduction band with the holes of the
398 core band. This recombination competes with the CVL. Nevertheless, in [34] an ultra-fast scintillation
399 mechanism (< 1 ns), ascribed to the CVL, was actually measured in a BaF₂ crystal after heavy ion
400 irradiation.

401 Finally, the optical filtration operated well in the case of the RL and TCSPC experiments, but no effects
402 were observed during the fast PMT experiments. Two possible explanations are 1) a problem in the
403 measurement setup, *i.e.* inaccurate coupling between crystal and filter, or 2) effects of the optical
404 grease and/or direct coupling between crystal and filter. The second hypothesis is related to the fact
405 that the dichroic filter used is slightly sensitive to both the impinging photon direction and the
406 refractive index of the medium it is in contact with. The filter transmittance was measured in air (figure
407 3), while during the measurements with the PMT the filter was in between the PMT and CLYC and its
408 surfaces were covered by the optical grease. Further investigations are required, in particular in the
409 light of performing n/γ discrimination using the emission-wavelength information.

410 **4. Conclusions**

411 The different experiments performed using the ⁷Li enriched crystal and the Asahi optical filter allowed
412 precisely characterizing the material scintillation process. The wavelength-resolved RL results
413 obtained with different photon energies allowed verifying that there is no LET-dependence of the CLYC
414 emission in the range 0.5–5 keV/ μ m, *i.e.* X-ray and γ -ray stimulations do not significantly distort the
415 CLYC scintillation process.

416 The fast PMT measurements allowed observing the effects of the neutron quenching in the time
417 domain. Differently from what reported by some authors: 1) a residual CVL signal is observed; 2) the
418 direct electron-hole capture is fully quenched by the neutron capture products. The fast characteristic
419 time and the rather flat quantum efficiency of the PMT allowed distinguishing among the fast and
420 ultra-fast mechanisms also in the presence of a strong CVL quenching.

421 The TCSPC measurements allowed validating the fast PMT findings. Moreover, the filtered vs
422 unfiltered TCSPC experiments suggested that in the 250–330 nm region both the CVL and the host
423 luminescence are present, with a predominant contribution due to the STE de-excitation. However,
424 the relative intensity of these two mechanisms cannot be precisely estimated because of the
425 uncertainty affecting the STE estimation and the short integration window of the TCSPC experiment.

426 **Acknowledgements**

427 We wish to thank Etiennette Auffray for putting at our disposal the equipment of the Crystal
428 Clear/EP_CMX_DA group for study of the scintillation properties. We also would like to thank the team
429 at FBK for their support and related material used in this study. This project has been partially funded
430 by the CERN Knowledge Transfer fund, through a grant awarded in 2014.

431 **References**

- 432 [1] J. Glodo, R. Hawrami, K.S. Shah, Development of Cs₂LiYCl₆ scintillator, *Journal of Crystal*
433 *Growth*. 379 (2013) 73–78. <https://doi.org/10.1016/j.jcrysgro.2013.03.023>.
- 434 [2] J. Glodo, W.M. Higgins, E. V.D. Van Loef, K.S. Shah, Scintillation properties of 1 inch
435 Cs₂LiYCl₆:Ce crystals, *IEEE Transactions on Nuclear Science*. 55 (2008) 1206–1209.
436 <https://doi.org/10.1109/TNS.2007.913467>.
- 437 [3] N. Dolympia, P. Chowdhury, E.G. Jackson, C.J. Lister, Fast neutron response of ⁶Li-depleted

- 438 CLYC detectors up to 20 MeV, *Nuclear Instruments and Methods in Physics Research, Section*
439 *A: Accelerators, Spectrometers, Detectors and Associated Equipment*. 763 (2014) 433–441.
440 <https://doi.org/10.1016/j.nima.2014.06.074>.
- 441 [4] N. Dinar, D. Celeste, M. Silari, V. Varoli, A. Fazzi, Pulse shape discrimination of CLYC scintillator
442 coupled with a large SiPM array, *Nuclear Instruments and Methods in Physics Research, Section*
443 *A: Accelerators, Spectrometers, Detectors and Associated Equipment*. 935 (2019) 35–39.
444 <https://doi.org/10.1016/j.nima.2019.04.099>.
- 445 [5] P.A. Rodnyi, Core-valence luminescence in scintillators, *Radiation Measurements*. 38 (2004)
446 343–352. <https://doi.org/10.1016/j.radmeas.2003.11.003>.
- 447 [6] N. D'Olympia, P. Chowdhury, C.J. Lister, J. Glodo, R. Hawrami, K. Shah, U. Shirwadkar, Pulse-
448 shape analysis of CLYC for thermal neutrons, fast neutrons, and gamma-rays, *Nuclear*
449 *Instruments and Methods in Physics Research, Section A: Accelerators, Spectrometers,*
450 *Detectors and Associated Equipment*. 714 (2013) 121–127.
451 <https://doi.org/10.1016/j.nima.2013.02.043>.
- 452 [7] R.H. Pots, E. Auffray, S. Gundacker, Exploiting Cross-Luminescence in BaF₂ for Ultrafast Timing
453 Applications Using Deep-Ultraviolet Sensitive HPK Silicon Photomultipliers, *Frontiers in Physics*.
454 8 (2020) 482. <https://doi.org/10.3389/fphy.2020.592875>.
- 455 [8] Z.W. Bell, D.E. Hornback, M.Z. Hu, J.S. Neal, Wavelength-based neutron/gamma ray
456 discrimination in CLYC, 2014 IEEE Nuclear Science Symposium and Medical Imaging
457 Conference, NSS/MIC 2014. (2016). <https://doi.org/10.1109/NSSMIC.2014.7431197>.
- 458 [9] B.S. Budden, L.C. Stonehill, J.R. Terry, A. V. Klimenko, J.O. Perry, Characterization and
459 investigation of the thermal dependence of Cs₂LiYCl₆: Ce³⁺ (CLYC) waveforms, *IEEE*
460 *Transactions on Nuclear Science*. 60 (2013) 946–951.
461 <https://doi.org/10.1109/TNS.2012.2215884>.
- 462 [10] D. Nesrine, Development of neutron detectors for use in radiation protection, University of
463 Paris-Saclay, 2019.
- 464 [11] E. V.D. Van Loef, P. Dorenbos, C.W.E. Van Eijk, K.W. Krämer, H.U. Güdel, Scintillation and
465 spectroscopy of the pure and Ce³⁺-doped elpasolites: Cs₂LiYX₆ (X = Cl, Br), *Journal of Physics*
466 *Condensed Matter*. 14 (2002) 8481–8496. <https://doi.org/10.1088/0953-8984/14/36/307>.
- 467 [12] P. Dorenbos, Scintillation mechanisms in Ce³⁺ doped halide scintillators, *Physica Status Solidi*
468 *(A) Applications and Materials Science*. 202 (2005) 195–200.
469 <https://doi.org/10.1002/pssa.200460106>.
- 470 [13] G. Zorloni, F. Cova, M. Caresana, M. Di Benedetto, J. Hostaša, M. Fasoli, I. Villa, I. Veronese, A.
471 Fazzi, A. Vedda, Neutron/γ discrimination by an emission-based phoswich approach, *Radiation*
472 *Measurements*. 129 (2019) 106203. <https://doi.org/10.1016/j.radmeas.2019.106203>.
- 473 [14] G. Zorloni, L. Cremonesi, F. Cova, A. Vedda, M. Caresana, Development of a new optical-based
474 quasi-digital particle discrimination technique using inorganic scintillators, *Radiation*
475 *Measurements*. 135 (2020) 106370. <https://doi.org/10.1016/j.radmeas.2020.106370>.
- 476 [15] M.N. Ullah, C. Park, E. Pratiwi, C. Kim, H. Choi, J.Y. Yeom, A new positron-gamma discriminating
477 phoswich detector based on wavelength discrimination (WLD), *Nuclear Instruments and*
478 *Methods in Physics Research, Section A: Accelerators, Spectrometers, Detectors and*
479 *Associated Equipment*. 946 (2019) 162631. <https://doi.org/10.1016/j.nima.2019.162631>.
- 480 [16] S. Gundacker, E. Auffray, K. Pauwels, P. Lecoq, Measurement of intrinsic rise times for various
481 L(Y)SO and LuAG scintillators with a general study of prompt photons to achieve 10 ps in TOF-

- 482 PET, *Physics in Medicine and Biology*. 61 (2016) 2802–2837. <https://doi.org/10.1088/0031-9155/61/7/2802>.
483
- 484 [17] S. Gundacker, R.M. Turtos, E. Auffray, P. Lecoq, Precise rise and decay time measurements of
485 inorganic scintillators by means of X-ray and 511 keV excitation, *Nuclear Instruments and
486 Methods in Physics Research, Section A: Accelerators, Spectrometers, Detectors and
487 Associated Equipment*. 891 (2018) 42–52. <https://doi.org/10.1016/j.nima.2018.02.074>.
- 488 [18] CLYC Gamma-Neutron Scintillator for SPRDs and RIIDs | RMD, Dynasil, (n.d.).
489 <https://www.dynasil.com/product-category/scintillators/clyc-gamma-neutron-scintillators/>
490 (accessed May 17, 2021).
- 491 [19] Optical Filters and Instruments | Asahi Spectra USA Inc., (n.d.). [https://www.asahi-](https://www.asahi-spectra.com/)
492 [spectra.com/](https://www.asahi-spectra.com/) (accessed May 17, 2021).
- 493 [20] Prime™ X, 2011. www.bwtek.com (accessed May 17, 2021).
- 494 [21] ISO 4037-1:2019, Radiological protection — X and gamma reference radiation for calibrating
495 dosimeters and doserate meters and for determining their response as a function of photon
496 energy., (n.d.).
- 497 [22] HAMAMATSU H6610, (n.d.). <https://dtsheet.com/doc/749739/hamamatsu-h6610> (accessed
498 May 17, 2021).
- 499 [23] PHOTOMULTIPLIER TUBES AND ASSEMBLIES FOR SCINTILLATION COUNTING & HIGH ENERGY
500 PHYSICS, (n.d.).
- 501 [24] F. Anghinolfi, P. Jarron, F. Krummenacher, E. Usenko, M.C.S. Williams, NINO, an ultra-fast, low-
502 power, front-end amplifier discriminator for the Time-Of-Flight detector in ALICE experiment,
503 in: *IEEE Nuclear Science Symposium Conference Record*, Institute of Electrical and Electronics
504 Engineers Inc., 2003: pp. 375–379. <https://doi.org/10.1109/nssmic.2003.1352067>.
- 505 [25] A. Gola, F. Acerbi, M. Capasso, M. Marcante, A. Mazzi, G. Paternoster, C. Piemonte, V.
506 Regazzoni, N. Zorzi, NUV-sensitive silicon photomultiplier technologies developed at
507 fondazione Bruno Kessler, *Sensors* (Switzerland). 19 (2019).
508 <https://doi.org/10.3390/s19020308>.
- 509 [26] Introduction to SiPM TECHNICAL NOTE, 2011.
- 510 [27] S. Gundacker, R.H. Pots, A. Nepomnyashchikh, E. Radzhabov, R. Shendrik, S. Omelkov, M. Kirm,
511 F. Acerbi, M. Capasso, G. Paternoster, A. Mazzi, A. Gola, J. Chen, E. Auffray, Vacuum ultraviolet
512 silicon photomultipliers applied to BaF₂ cross-luminescence detection for high-rate ultrafast
513 timing applications , *Physics in Medicine & Biology*. 66 (2021) 114002.
514 <https://doi.org/10.1088/1361-6560/abf476>.
- 515 [28] S. Lam, J. Fiala, M. Hackett, S. Motakef, A High-Performance CLYC(Ce)-PVT Composite for
516 Neutron and Gamma Detection, *IEEE Transactions on Nuclear Science*. 65 (2018) 609–615.
517 <https://doi.org/10.1109/TNS.2017.2779783>.
- 518 [29] No Title, (n.d.). <https://physics.nist.gov/PhysRefData/Star/Text/ESTAR.html> (accessed August
519 18, 2021).
- 520 [30] G.F.Knoll, *Radiation Detection and Measurements*, 4th ed., 2010.
- 521 [31] X. Wen, A. Enqvist, Measuring the scintillation decay time for different energy deposited by γ -
522 rays and neutrons in a Cs₂LiYCl₆:Ce³⁺ detector, *Nuclear Instruments and Methods in Physics
523 Research, Section A: Accelerators, Spectrometers, Detectors and Associated Equipment*. 853
524 (2017) 9–15. <https://doi.org/10.1016/j.nima.2017.02.019>.

- 525 [32] C.M. Combes, P. Dorenbos, C.W.E. Van Eijk, K.W. Krämer, H.U. Güdel, Optical and scintillation
526 properties of pure and Ce³⁺-doped Cs₂LiYCl₆ and Li₃YCl₆: Ce³⁺ crystals, *Journal of*
527 *Luminescence*. 82 (1999) 299–305. [https://doi.org/10.1016/S0022-2313\(99\)00047-2](https://doi.org/10.1016/S0022-2313(99)00047-2).
- 528 [33] M. Kirm, A. Lushchik, C. Lushchik, A.I. Nepomnyashikh, F. Savikhin, Dependence of the
529 efficiency of various emissions on excitation density in BaF₂ crystals, *Radiation Measurements*.
530 33 (2001) 515–519. [https://doi.org/10.1016/S1350-4487\(01\)00044-0](https://doi.org/10.1016/S1350-4487(01)00044-0).
- 531 [34] K. Kimura, LET-, ionic species- and temperature-dependence on Auger-free and self-trapped
532 exciton luminescence of ion-irradiated BaF₂ and CsCl single crystals, *Nuclear Instruments and*
533 *Methods in Physics Research Section B: Beam Interactions with Materials and Atoms*. 116
534 (1996) 57–60. [https://doi.org/https://doi.org/10.1016/0168-583X\(96\)00011-0](https://doi.org/https://doi.org/10.1016/0168-583X(96)00011-0).
- 535